JAMEA

JOURNAL OF ADVANCED MECHANICAL ENGINEERING APPLICATIONS
e-ISSN: 2716-6201

Vol. 7 No. 1 (2026) 115-128
https://publisher.uthm.edu.my/ojs/index.php/jamea

Hemodynamic Efficacy of Flow Diverter Stents in Intracranial Aneurysms: A Computational Analysis of Wall Shear Stress

Muhammad Affiq Syukri Arafat[1], Nor Adrian Nor Salim[1*], Nur Amani Hanis Roseman[1]

[1] *Department of Mechanical Engineering, Faculty of Mechanical Engineering and Manufacturing, Universiti Tun Hussein Onn Malaysia, Parit Raja, Batu Pahat, 86400, Johor, MALAYSIA*

*Corresponding Author: adrian@uthm.edu.my
DOI: https://doi.org/10.30880/jamea.2026.07.07

Article Info

Received: 2 March 2026
Accepted: 28 May 2026
Available online: 30 June 2026

Keywords

Intracranial aneurysm, flow diverter stent, computational fluid dynamics (CFD), time-averaged wall shear stress (TAWSS)

Abstract

Intracranial aneurysms (IAs) pose a severe clinical risk of catastrophic rupture, a life-threatening event largely driven by continuous and localized hemodynamic forces acting upon the structurally weakened arterial wall. While the deployment of flow diverter (FD) stents has emerged as a highly effective endovascular intervention to disrupt intra-aneurysmal flow, determining the most mechanically protective stent configuration remains a significant challenge. Suboptimal deployment can inadvertently worsen local shear stresses, exacerbate endothelial dysfunction and accelerate vascular degradation. Therefore, this study aims to evaluate the hemodynamic efficacy of various FD stent configurations by analyzing their impact on Time-Averaged Wall Shear Stress (TAWSS) distributions—specifically physiological $\mathrm{TAWSS}_{\mathrm{normal}}$, stagnated $\mathrm{TAWSS}_{\mathrm{low}}$, and critical $\mathrm{TAWSS}_{\mathrm{high}}$ shear regions to identify designs that best mitigate rupture risks. Computational hemodynamic analysis revealed varying degrees of efficacy across the tested configurations. A hemodynamically ideal stent must promote $\mathrm{TAWSS}_{\mathrm{normal}}$ to maintain endothelial homeostasis, while strictly minimizing $\mathrm{TAWSS}_{\mathrm{low}}$, which triggers inflammatory pathways, and $\mathrm{TAWSS}_{\mathrm{high}}$ (> 10 Pa), which drives destructive extracellular matrix degradation via matrix metalloproteinases (MMPs). Among the evaluated designs, Model 5 demonstrated the most optimal and highly protective mechanical profile. It successfully suppressed the $\mathrm{TAWSS}_{\mathrm{high}}$ luminal coverage area to merely 0.361%, effectively dampening the incoming high-velocity blood jets and balancing the overall shear distribution far better than the untreated baseline and other configurations. These findings emphasize that selecting the optimal FD stent geometry is crucial for restoring physiological hemodynamics and preventing post-treatment hemorrhagic rupture, providing essential insights for future neurovascular stent designs.

1. Introduction

Intracranial aneurysms (IAs) are a cerebrovascular condition characterized by the abnormal dilation of a weakened cerebral artery wall. This structural degradation occurs when the middle and inner layers of the arterial wall deteriorate, leading to a reduction in the smooth muscle cells responsible for maintaining vascular integrity [1], [2]. If left untreated, continuous hemodynamic forces on this fragile sac can lead to rupture, resulting in subarachnoid hemorrhage, a medical emergency associated with high rates of morbidity and mortality. In recent years, endovascular interventions have improved the management of IAs, providing an alternative to invasive open surgical clipping. Among these strategies, the deployment of flow diverter (FD) stents has emerged as an effective treatment, especially for complex, wide necked, or giant saccular aneurysms that are challenging to treat conventional micro coiling [3].

The working principle of a flow diverter stent is based on its ability to alter the local hemodynamic environment of the diseased vessel. Unlike conventional stents that act mainly as a structural scaffold, flow diverters are woven with a high metal surface coverage ratio and low porosity. When deployed across the aneurysm neck, this metallic mesh acts as a mechanical barrier that separates the blood flow in the parent artery from the circulation within the aneurysm sac. This flow disruption reduces the kinetic energy and momentum of the blood entering the dome, inducing a state of hemodynamic stasis[4]. This flow stagnation promotes gradual intra aneurysmal thrombosis, encourages endothelial cell proliferation across the stent struts, and leads to the occlusion and healing of the aneurysm [5].

Therefore, understanding the fluid dynamics surrounding the stent is essential for evaluating its biomechanical efficacy. Hemodynamic forces, primarily Wall Shear Stress (WSS), which is the frictional force exerted by flowing blood on the vessel wall, are the primary stimuli governing the initiation, growth, and rupture of IAs. Because the cerebral cardiac cycle is pulsatile, blood flow velocity and WSS are transient phenomena that fluctuate over time. To capture these temporal variations, Time Averaged Wall Shear Stress (TAWSS) is utilized as a fundamental metric. TAWSS consolidates the dynamic shear stress variations over an entire cardiac cycle into a single spatial map, identifying regions vulnerable to vascular wall remodeling [6], [7].

Although the reduction of intra aneurysmal flow velocity and overall WSS after stenting indicates treatment success, localized spatial variations in shear stress remain complex. The presence of metallic stent struts introduces heterogeneous flow patterns within the parent artery and at the aneurysm neck. This creates distinct shear stress zones that influence clinical outcomes; certain stress regimes facilitate thrombosis and healing, while extreme deviations can pose risks of complications such as in stent stenosis or branch artery occlusion [3], [8]. Therefore, relying only on average global WSS values is insufficient. A localized categorization of these stress zones is necessary for a complete biomechanical assessment of the stent performance.

Previous foundational research established a reliable computational framework for the hemodynamic analysis of an idealized untreated aneurysm model. Building upon those foundational findings, the current research integrates a flow diverter stent intervention into that exact simulated environment. This direct continuation provides a reliable comparative baseline [9]. Utilizing a previously established model helps in isolating the specific mechanical effects of the stent on the localized fluid dynamics without introducing new geometric variables. Therefore, extending this prior work allows for a highly controlled evaluation of how the intervention redistributes shear stress across the vascular walls [6].

This study aims to visualize and quantify the TAWSS parameter classifications, specifically mapping the low, normal (norm), and high TAWSS regimes within a computational intracranial aneurysm model treated with a flow diverter stent. By analyzing these hemodynamic parameters, this research provides a quantitative understanding of the stent performance. Correlating these TAWSS classifications with expected biological responses offers insights into the impact of the stent on aneurysm hemodynamics, contributing to predictive models for clinical success.

The previous computational fluid dynamics (CFD) studies have extensively explored the general efficacy of flow diverter stents. However, the majority of these investigations focus on global flow reduction rather than the localized shifts between specific physiological and pathological shear stress thresholds. Furthermore, this study builds upon our previous work on hemodynamic analysis of intracranial aneurysms [15]. Our prior investigations focused primarily on velocity profile, pressure distribution, wall shear stress (WSS), oscillatory shear index (OSI) and relative residence time (RRT); in contrast, the present study advances this field by systematically quantifying the proportional shift of aneurysm surface area into distinct TAWSS zones (low, normal, and high) across multiple stent configurations. This targeted approach provides a more granular understanding of how different stent configurations redistribute wall shear stress, offering quantitative insights that aid in optimizing stent selection.

J. Adv. Mech. Eng. Appl. Vol. 7 No. 1 (2026) p. 115-128

2. Methodology

This computational investigation was conducted by adopting the simulation framework from a previous baseline study. A standard computational fluid dynamics study is systematically divided into three primary phases: preprocessing, solving, and postprocessing. The preprocessing stage is dedicated to preparing the computational model prior to execution. This phase involves constructing the specific aneurysm geometry, generating the mesh, defining the boundary conditions, and selecting appropriate physical models to represent the blood flow. Subsequently, the solving stage entails configuring the numerical solver. This requires selecting the solver type, applying spatial discretization methods, establishing convergence criteria, and determining precise time step settings to accurately capture the pulsatile flow. Finally, the postprocessing phase extracts and visualizes the resulting hemodynamic data [8]. Overall, these simulation methodologies were structured based on established protocols to ensure validity and accuracy.

2.1 Governing Equation

The resolution of fluid dynamics within the computational model relies on the continuity and Navier Stokes equations, which govern the motion of incompressible fluids. These equations are essential for accurately detailing flow behaviour across complex anatomical geometries, especially those complicated by the presence of intravascular stents.

The numerical simulations were conducted assuming a laminar flow regime. This condition is highly suitable for the low Reynolds number environment typical of blood flow in small cerebral arteries, allowing for the direct resolution of the equations without the need for additional turbulence modelling. Consequently, the conservation of mass and momentum is represented by the incompressible continuity and Navier Stokes equations, formulated as Equation 1 and Equation 2 [10], [11]:

$$\nabla.(\vec{v}) = 0 \tag{1}$$

$$\rho\left(\frac{\partial \vec{v}}{\partial t} + \vec{v}.\nabla\vec{v}\right) = -\nabla p + \mu\nabla^2\vec{v} + \vec{F} \tag{2}$$

Where ν represents the velocity vector, ρ is fluid density p is the fluid pressure, μ is dynamic viscosity and F represent body forces.

2.2 Hemodynamic Parameter of Intracranial Artery

Multiple hemodynamic indicators were utilized to assess how morphological variations influence the formation of atherosclerosis-prone regions in intracranial arteries.

2.2.1 Time Averaged Wall Shear Stress (TAWSS)

The hemodynamic environment of intracranial arteries is critical to their structural and functional integrity, with Time-Averaged Wall Shear Stress (TAWSS) serving as a key indicator. Wall Shear Stress (WSS), defined as the tangential frictional force exerted by blood flow on the arterial endothelium, is instrumental in predicting vascular remodelling and disease progression. The magnitude of WSS can be quantified using various formulations. Under idealized laminar flow, it is given by Poiseuille's law as written in Equation 3, which relates WSS to blood's dynamic viscosity, μ_d, flow rate, Q and the arterial radius, r. A more general definition, applicable in complex geometries, derives WSS from the fluid viscous stress tensor (τ_{ij}) as expressed in Equation 4 [12], [13]:

$$\tau_w = \frac{4\mu_d Q}{\pi r^3} \tag{3}$$

$$\tau_w = t - (t \cdot n)n \tag{4}$$

Aberrant WSS values within the cerebral vasculature are linked to distinct pathologies. Specifically, low WSS values of less than 1 Pa promote an atherogenic endothelial phenotype, increasing susceptibility to atherosclerosis. In contrast, high WSS values exceeding 7 Pa can lead to endothelial dysfunction and a heightened risk of thrombotic events or plaque erosion. The physiological range for healthy intracranial arteries is generally accepted to be between 1 and 7 Pa [6]. Since cerebral blood flow is inherently pulsatile, a time-averaged value is required for meaningful analysis. TAWSS is therefore computed by integrating the instantaneous WSS magnitude, $|\tau_w|$, over the period of one full cardiac cycle, T, as shown in Equation 5 [14]:

$$TAWSS = \frac{1}{T}\int_{0}^{T} |\vec{\tau}_w| \, dt \tag{5}$$

2.3 Simplified Geometry Model

The previous analysis utilized a specifically developed three-dimensional geometry that represents an idealized intracranial saccular aneurysm. The baseline model was constructed using SolidWorks 2023 computer aided design software and subsequently imported into ANSYS Fluent 2023 DesignModeler for preprocessing and simulation setup [15].

Six distinct computational models were employed in this research for the comprehensive evaluation of hemodynamic performance. Fig. 1 illustrates the simplified geometry of the first configuration, designated as Model 1, which includes the parent artery and the saccular dome. Model 1 served as the baseline or untreated aneurysm geometry without any stent deployment. The structural geometry consists of a straight parent artery modelled as a cylinder with a uniform diameter of 4 mm and a total length of 50 mm. A saccular aneurysm with a maximum dome diameter of 10 mm and a neck width of 7.55 mm is positioned along the wall of the parent vessel, accurately reflecting the typical morphology associated with this vascular condition [15].

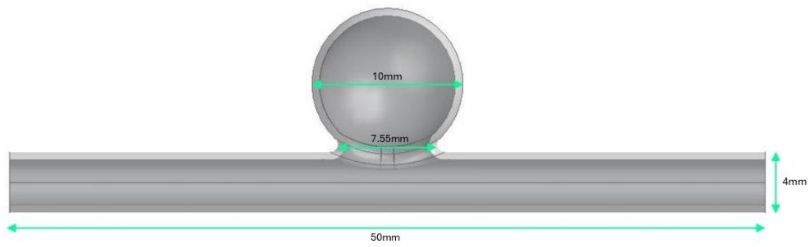

Fig. 1 *Geometry of simplified intracranial artery with Aneurysms model (Model 1)*

Virtual deployment of five distinct stent geometries within the idealized aneurysm model was executed during the simulation phase, yielding five complete computational configurations designated as (a) through (e) in Fig. 3. As shown in Fig. 2, these stents were strategically positioned to span the 7.55 mm neck width, replicating a clinical procedure where the device acts as a scaffold diverting blood flow away from the sac. Maintaining a constant aneurysm and parent vessel morphology across all six simulations ensures that any variations in hemodynamic parameters, such as intra aneurysmal flow velocity, pressure distribution, and wall shear stress, are directly attributable to the specific geometric design of the stent. This methodological consistency guarantees a rigorous and unbiased assessment of the therapeutic performance for each device [16].

Specific dimensional specifications for each stent utilized throughout this research are detailed in Table 1. All stent models share an identical diameter of 3.05 mm and a wall thickness of 0.13 mm, ensuring a consistent radial profile across all configurations. The stent length was intentionally varied from Model 2 through Model 6 for systematically investigating the influence of landing zone coverage on intra aneurysmal hemodynamic. Model 2 represents the minimum functional length required for covering the aneurysm neck, while the subsequent models incorporate incrementally longer devices that extend the proximal and distal landing zones within the parent artery. This progressive length variation facilitates a comprehensive assessment regarding how flow straightening upstream of the aneurysm influences diversion efficiency, ultimately determining whether extended vascular coverage provides a superior reduction of the aneurysmal inflow jet [15], [17].

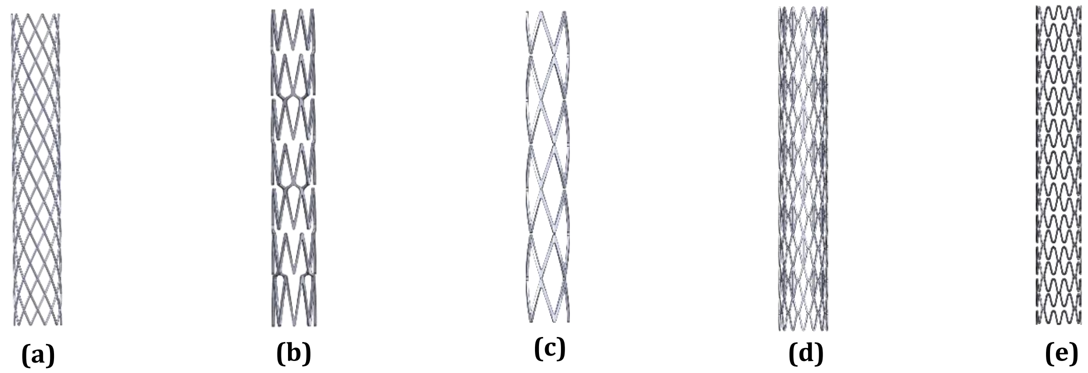

Fig. 2 *Geometry for 5 types of stents (a) Type 1; (b) Type 2; (c) Type 3; (d) Type 4; (e) Type 5*

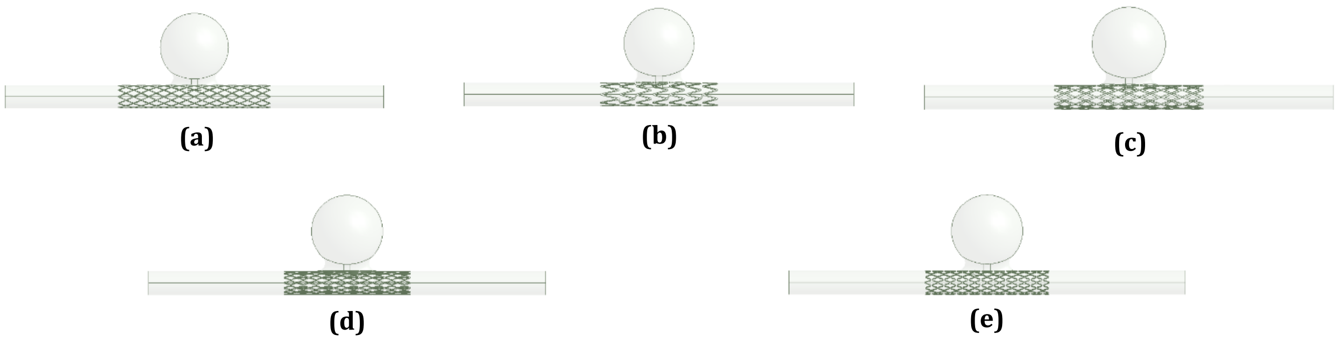

Fig. 3 *Geometry for the five stent-aneurysm configurations (a) Model 2; (b) Model 3; (c) Model 4; (d) Model 5; (e) Model 6*

Table 1 *Specification for each stent*

Type of stent	Diameter (mm)	Length (mm)	Thickness
Type 1	3.05	18.20	0.13
Type 2	3.05	17.05	0.13
Type 3	3.05	15.05	0.13
Type 4	3.05	15.90	0.13
Type 5	3.05	15.90	0.13

2.4 Discretization Technique

The computational domains were discretized utilizing unstructured tetrahedral elements for accurately capturing the intricate arterial geometry and the explicit substructure of the flow diverter stents. This methodological approach was selected for resolving complex hemodynamic features, which include velocity gradients and wall shear stress within critical regions. The meshing strategy prioritized solution accuracy by applying curvature-based refinement in areas characterized by high geometric complexity, particularly surrounding the aneurysm neck and the stent struts [13].

Across all six configurations, mesh density was rigorously optimized for ensuring grid independence and capturing boundary layer flow accurately. Model 1 utilized 371,180 nodes and 1,194,212 elements with a fine element size of 0.13 mm, enabling a precise representation of the geometric features. For the stented configurations spanning Models 2 through 6, the physical presence of the stent struts necessitated further local refinement for resolving flow separation around the metallic wires. Model 2 employed a mesh consisting of 1,462,869 nodes and 4,876,818 elements with a base element size of 3.05 mm, providing adequate resolution of global flow patterns while simultaneously managing computational demand. This specific model featured a dense stent configuration that ultimately comprised 4.8 million elements, utilizing a global maximum size of 0.20 mm alongside a highly refined sizing of approximately 0.02 mm near the stent wires for capturing micro flow dynamics. The variation in node counts across the subsequent models fundamentally reflects the geometric differences in stent coverage rather than any inconsistent meshing standards. Model 3 was constructed with

424,516 nodes and 1,406,535 elements at an element size of 2.50 mm, whereas Model 4 utilized 342,721 nodes and 1,131,613 elements with a smaller element size of 1.75 mm for improving accuracy in regions exhibiting higher curvature. Furthermore, Model 5 contained 353,377 nodes and 1,872,135 elements at an element size of 2.50 mm, and Model 6 comprised 931,676 nodes and 3,077,746 elements using the identical 2.50 mm element size, offering a refined resolution highly suitable for rigorous hemodynamic evaluation [15].

The finalized computational meshes exhibited exceptionally high quality, yielding an average skewness of 0.28115 alongside an orthogonal quality of 0.97285. These specific metrics greatly surpass the recommended criteria established for cardiovascular simulations within ANSYS Fluent. As depicted in Fig. 4(a), the mesh structure transitions smoothly from the central core flow toward the solid wall boundaries. Accurate resolution of near wall velocity gradients was achieved by generating inflation layers consisting of five boundary layers situated along the arterial wall and stent surfaces, which is visually depicted in Fig. 4(b). Fig. 4(b) additionally illustrates the detailed mesh refinement executed around the stent struts, ensuring the precise detection of low shear zones inherently associated with elevated thrombosis risks[18].

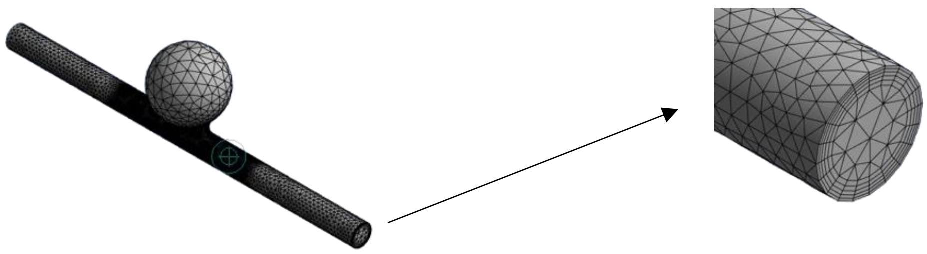

(a) **(b)**

Fig. 4 *Tetrahedral meshing for all intracranial artery over all the stents (a) Body sizing; and (b) Inflation*

Conducting a Grid Independence Test for the Type 3 stent in Model 4 was required for ensuring that the computational fluid dynamics simulation results remained entirely independent of mesh density. This crucial validation step confirmed the accuracy and overall robustness of the numerical model. Systematic mesh refinement was executed across five distinct configurations, which are detailed in Table 2. The evaluated mesh densities ranged from a coarse setup designated as GIT 1 containing approximately 716,000 elements, scaling up to a highly refined mesh labeled GIT 5 that exceeded 1.2 million elements. Determining the optimal mesh resolution capable of producing stable numerical results while preserving computational efficiency was the primary objective of this procedure [19].

The velocity profiles extracted from these evaluated configurations are visually presented in Fig. 5, the TAWSS along a predefined line on the aneurysm dome was compared across the grids demonstrating a consistent and clear convergence pattern. Although the course meshes of GIT 1 and GIT 2 exhibited noticeable variations in their resultant profiles, the data generated by GIT 3 closely aligned with the highly refined outputs of GIT 4 and GIT 5. Grid independence was successfully achieved at the GIT 3 level, evidenced by the marginal difference in WSS between GIT 3 and the denser meshes remaining strictly below 1.5 %. Consequently, the GIT 3 configuration was definitively selected as the optimal computational setup, providing an ideal balance between strict solution accuracy and acceptable computational cost [15].

Table 2 *Parameter used in GIT for model 3*

Parameter	GIT 1	GIT 2	GIT 3	GIT 4	GIT 5
Element size	4.00 mm	3.50 mm	3.05 mm	1.75 mm	0.30 mm
Number of nodes	223134	249131	280105	342721	374981
Number of elements	715927	809353	916877	1131613	1226306

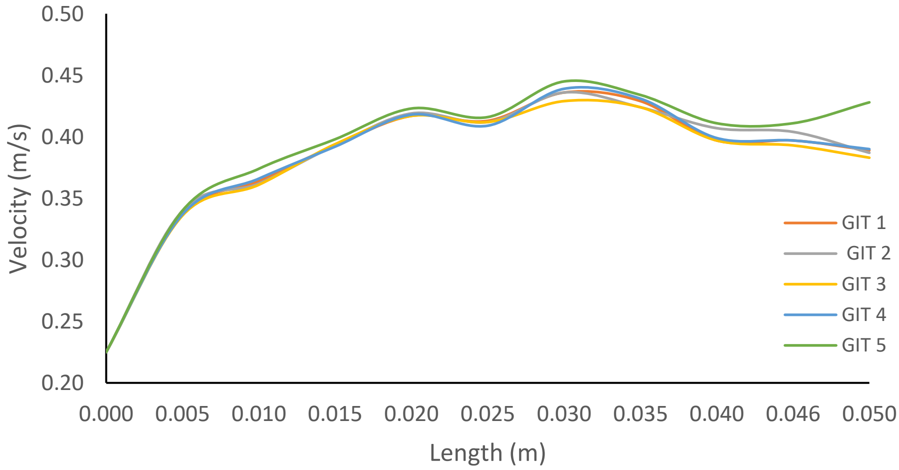

Fig. 5 *GIT chart using type 3 stent configuration in simplified model*

2.5 Boundary Conditions and Parameter Assumptions

This numerical investigation simulated the hemodynamic behavior within a stented intracranial artery segment by establishing transient and incompressible flow conditions. A laminar flow regime was designated for the simulation, justified by the low Reynolds number characteristically observed in arteries of this anatomical scale, which definitively remains below the critical threshold for turbulence. Securing a physiologically relevant representation required modeling the blood with a constant density of 1055 kg/m^3. While blood naturally exhibits non-Newtonian characteristics, its rheological properties were practically simplified in this study by assigning a constant dynamic viscosity of 0.004 Pa·s [18].

The inlet boundary condition involved applying a time dependent pulsatile velocity profile for accurately representing the dynamic flow within the intracranial artery. This specific approach successfully captures the physiological time dependent variation of blood velocity induced by the cardiac cycle within a rigid cylindrical vessel. The resulting solution effectively accounts for fluid viscosity and pulsation frequency, yielding a velocity distribution that continuously varies in magnitude and radial shape throughout the entire cycle. A simplified sinusoidal waveform was applied for approximating the cardiac cycle. Fig. 6 illustrates the temporal variation of this inlet condition over two complete cardiac cycles totalling 2 seconds. A fixed step size of 0.02 seconds was utilized for resolving the transient variations across the pulsatile blood flow simulation. Ensuring numerical stability and solution convergence requires configuring the solver to execute a minimum of five iterations per time step prior to advancing toward the subsequent time level. The prescribed velocity systematically fluctuates between a diastolic minimum of approximately 0.18 m/s and a systolic maximum of nearly 0.30 m/s, resulting in a mean time averaged value of 0.25 m/s [20].

Rigid no slip boundary conditions were strictly imposed upon the arterial walls and stent surfaces, thereby ensuring absolute zero velocity at all fluid solid outlet boundaries. Gravitational effects were considered entirely negligible when compared directly against the prescribed inlet velocity and outlet pressure magnitudes. These combined assumptions enabled the computational setup to provide a physiologically consistent representation of the transient laminar blood flow within the intracranial artery. This framework allowed for a highly detailed assessment regarding wall shear stress patterns associated directly with the presence of the stent. Resolving the complex pressure velocity coupling was achieved by implementing the coupled algorithm within ANSYS Fluent, which systematically updates both variables simultaneously during each iteration step. Adopting this rigorous numerical approach guaranteed robust convergence while significantly enhancing the predictive accuracy regarding the hemodynamic environment and shear stress characteristics within the stented vessel [21], [22].

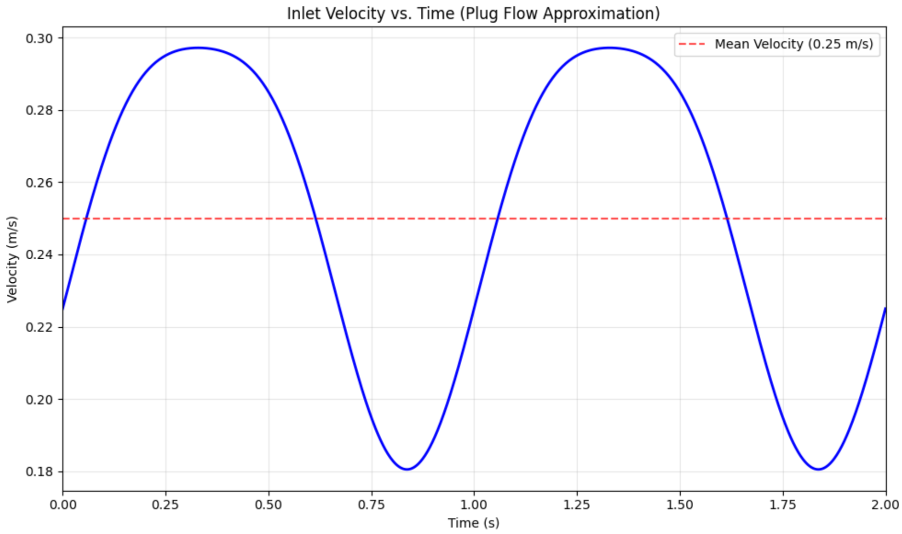

Fig. 6 *Sinusoidal inlet velocity profile with a mean of 0.25 m/s*

3. Results

The subsequent sections detail the findings derived from the computational analysis, which was executed for evaluating the hemodynamic characteristics of blood flow within intracranial aneurysms managed across various stent configurations and deployment strategies. The post processing analysis focused on extracting the frictional force parameters acting on the vessel walls, specifically breaking down the variations in shear stress induced by the intervention.

3.1 Time Averaged Wall Shear Stress (TAWSS) Distribution on Intracranial Aneurysms

Vascular hemodynamic behavior across the various simulated conditions is characterized by the Time Averaged Wall Shear Stress (TAWSS) distributions across an unstented baseline aneurysm Model 1 and five variations of stented geometries (Models 2 to 6), as shown in Fig. 7. Within the unstented control Model 1, the straight parent artery exhibits physiological TAWSS values ranging primarily between 2.90 Pa and 3.20 Pa. In contrast, a critical focal elevation of TAWSS, reaching peak values of approximately 4.70 Pa to 5.00 Pa, is distinctly observed at the distal neck of the aneurysm owing to direct flow impingement from the parent vessel. Meanwhile, the main dome of the aneurysm is subjected to a characteristically low shear environment, with values predominantly hovering near the minimum scale limit of 2.00 Pa to 2.30 Pa, reflecting a zone of flow stagnation typical of such saccular vascular pathologies.

The deployment of flow diverting stents in Models 2 to 6 demonstrates a profound and unified modification of the hemodynamics within the aneurysm. Across all observed stent configurations, the critically elevated TAWSS previously concentrated at the distal impingement zone in Model 1 is successfully mitigated and dissipated. This reduction provides crucial mechanical protection to the fragile aneurysm neck, lowering the risk of rupture. Furthermore, the stented models successfully maintain the uniformly low shear environment within the entirety of the aneurysm sac (remaining consistently at ≤ 2.30 Pa). This global reduction of shear stress inside the dome is a highly desirable clinical outcome, as it promotes blood flow stasis and accelerates the formation of stable thrombosis inside the aneurysm, which serves as the primary therapeutic mechanism for endovascular stenting.

In addition to TAWSS mapping, analysis of the velocity streamlines reveals that the unstented model exhibits a strong inflow jet impinging directly on the distal neck. Following the deployment of the FD stent, the velocity vectors within the aneurysm sac are markedly diminished. Despite the highly beneficial hemodynamic alterations achieved within the aneurysm sac, the introduction of the stent structures induces significant localized adverse effects within the parent vessel. A detailed numerical analysis of the stented Models 2 to 6 reveals marked focal spikes in TAWSS distributed directly along the metallic struts and their structural intersections. Depending on the specific stent porosity and strut geometry, such as the closed cell diamond design in Model 4 or the dense braided structures in Model 2 and Model 6, the localized TAWSS on the struts frequently escalates to the maximum scale value of 5.00 Pa. These localized zones of extreme, non-physiological high shear stress are clinically concerning, as such elevated mechanical forces (≥ 4.70 Pa) can trigger endothelial cell damage, platelet activation, and subsequent neointimal hyperplasia, potentially increasing the long-term risk of restenosis within the stent [6], [23].

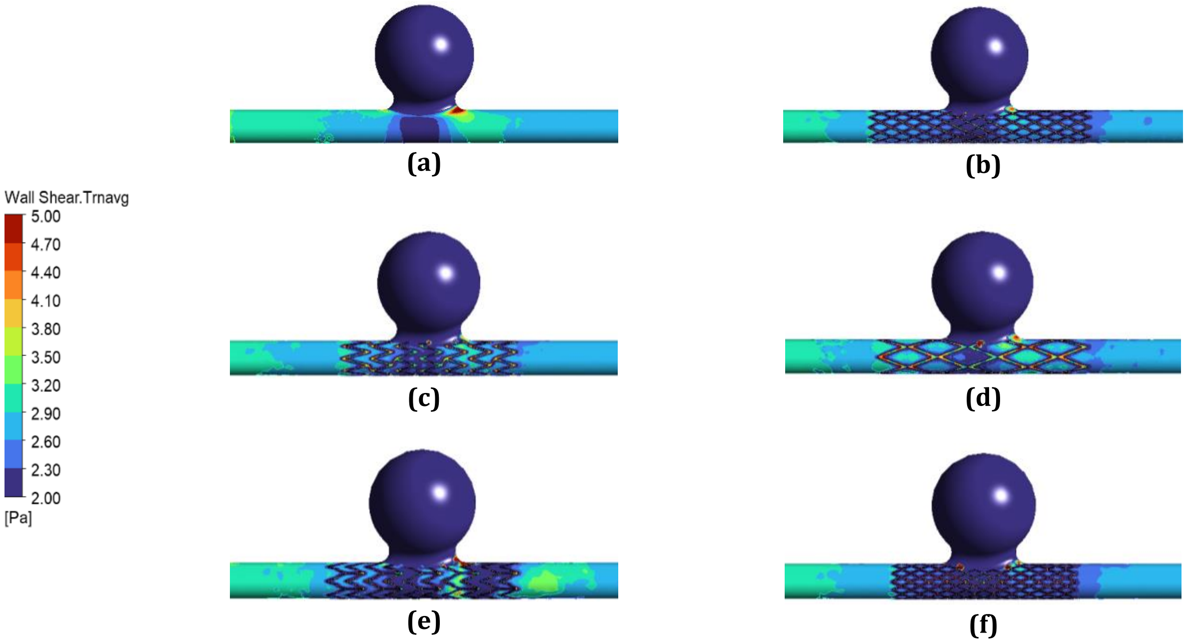

Fig. 7 *Time averaged-wall shear stress distribution for the six model of intracranial aneurysms (a) Model 1; (b) Model 2; (c) Model 3; (d) Model 4; (e) Model 5; (f) Model 6*

3.2 Percentage of Luminal Surface Area Exposed to TAWSS

The distribution of time-averaged wall shear stress (TAWSS) quantifies the average shear stress acting upon the luminal surface of intracranial arteries presenting with simplified aneurysmal geometries. To facilitate a more comprehensive investigation of the spatial area subjected to varying hemodynamic burdens, this parameter was further classified into three distinct categorical ranges: $TAWSS_{low}$, $TAWSS_{normal}$ and $TAWSS_{high}$. In the specific context of intracranial aneurysms, $TAWSS_{low}$ is defined as values lower than 0.4 Pa, whereas $TAWSS_{high}$ indicates values exceeding 10 Pa, and $TAWSS_{normal}$ encompasses the intermediate baseline range between 1.5 Pa and 4.0 Pa [6].

3.2.1 $TAWSS_{low}$

The systematic evaluation of the hemodynamic modulation achieved by the flow diverter configurations requires a quantitative assessment of the spatial distribution of low time-averaged wall shear stress ($TAWSS_{low}$ < 0.4 Pa) over the luminal surface area. Based on the numerical datasets extracted from the computational fluid dynamics simulations, as shown in Fig. 8, the untreated baseline configuration (Model 1) exhibited the highest surface area coverage at 34.523%. Among the stented models, Model 6 achieved the closest coverage to the baseline at 34.299%. Conversely, the remaining stent designs demonstrated marginally lower coverages, with Model 4, Model 2, and Model 3 exhibiting values of 33.383%, 33.366%, and 33.297%, respectively, while Model 5 recorded the lowest low-shear exposure at 33.222%.

Biomechanical principles dictate that the high $TAWSS_{low}$ area observed in the untreated Model 1 fundamentally represents the massive, naturally occurring pathological flow stagnation located deep within the wide aneurysmal dome before any intervention. Within the framework of endovascular therapy, the clinical objective of deploying a flow diverter is to replicate or enhance this hemodynamic stasis specifically within the aneurysmal sac [13]. When high-velocity inflows are sufficiently reduced by the stent struts, the resulting low shear stress states facilitate platelet aggregation and promote stable clot formation, which is the primary mechanism of curative aneurysm occlusion [24].

Consequently, evaluating the treated configurations reveals that Model 6 (34.299%) possesses a superior mechanical capacity to induce controlled hemodynamic stasis. By successfully mimicking the spatial reach of the baseline $TAWSS_{low}$ threshold, this specific stent design effectively shields the fragile vascular regions from persistent high-velocity inflow. This localized velocity reduction safely maintains the necessary blood stasis for thrombotic occlusion of the pathological sac without unnecessarily expanding low-shear zones into the healthy parent vessel [6], [25].

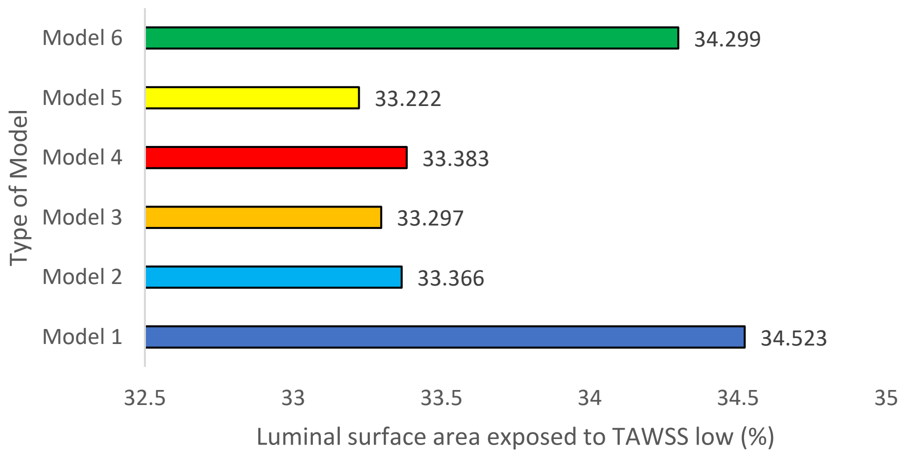

Fig. 8 *$TAWSS_{low}$ (TAWSS < 0.4 Pa) distribution coverage to luminal surface area of intracranial aneurysm model*

3.2.2 $TAWSS_{normal}$

The restoration of physiological baseline shear stress along the parent artery is imperative beyond inducing localized flow stasis within the aneurysmal region, which was analyzed using the normal range ($TAWSS_{normal}$ between 1.5 Pa and 4.0 Pa). The computational findings, as illustrated in Fig. 9, reveal that the untreated control configuration (Model 1) exhibited the highest baseline physiological shear surface area at 60.408%. Among the stented configurations, varying degrees of hemodynamic alteration were observed, with Model 3 and Model 4 achieving the highest physiological preservation at 57.783% and 56.352%, respectively. In contrast, a more pronounced reduction in normal physiological shear distribution was recorded in Model 2 (52.881%), Model 5 (52.845%), and Model 6 (50.302%).

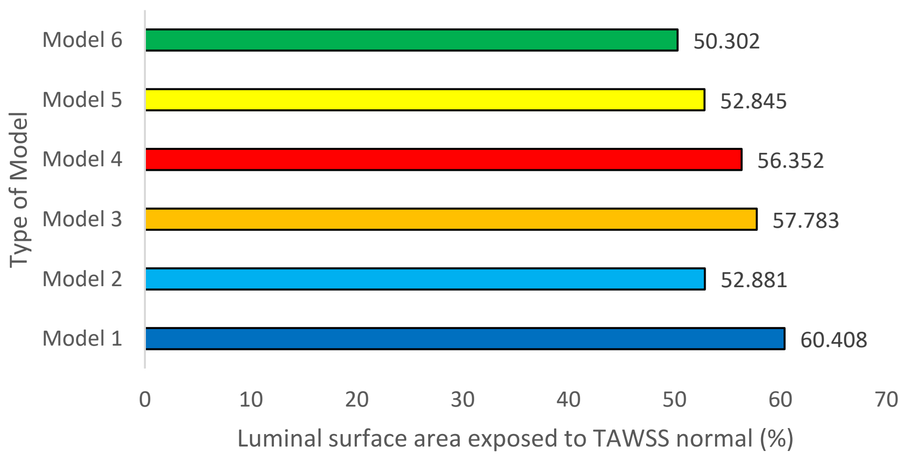

Fig. 9 *$TAWSS_{normal}$ (1.5 Pa≥ TAWSS ≥ 4.0 Pa) distribution coverage to luminal surface area of intracranial aneurysm model*

The established principles in vascular biology indicate that the high percentage of $TAWSS_{normal}$ in the untreated baseline (Model 1) represents the native homeostatic state of the healthy segments of the parent artery before endovascular intervention. Upon the deployment of flow diverter stents (Models 2 to 6), the physical presence of the stent mesh introduces a mechanical drag effect and localized flow disturbances along the arterial wall. This intervention inherently converts portions of the normal shear stress zones into low shear stress regions

$\mathrm{TAWSS_{low}}$, thereby explaining the global reduction in $\mathrm{TAWSS_{normal}}$ percentages across all treated models compared to the control.

Accordingly, the evaluation of the treated configurations demonstrates that Model 3 provides the most optimal balance in maintaining parental arterial health among the stented designs. By retaining 57.783% of the luminal surface area within the homeostatic shear stress window, Model 3 minimizes the adverse structural risk of over-dampening the wall shear stress along the parent vessel. Minimizing this reduction is vital for preventing endothelial cell dysfunction and mitigating long-term clinical complications such as intimal hyperplasia or in-stent restenosis, while simultaneously redirecting the pathological jet away from the aneurysm sac [6], [26].

3.2.3 $\mathbf{TAWSS}_{high}$

The rigorous quantification of the luminal surface area subjected to abnormally high shear stress ($\mathrm{TAWSS_{high}}$ > 10 Pa) provides a comprehensive evaluation of the potential risk of structural degradation and mechanical fatigue on the vessel wall. The resulting datasets, as presented in Fig. 10, highlight that the untreated baseline (Model 1) presents an inherent extreme shear exposure of 0.517%. Post-intervention, Model 5 demonstrated the most favorable biomechanical profile by significantly reducing this coverage to a minimum of 0.361%. In stark contrast, certain stented designs exacerbated the high-shear regions, with Model 6 and Model 4 recording elevated values of 0.620% and 0.571%, respectively, surpassing the baseline risk.

Pathophysiologically, the baseline $\mathrm{TAWSS_{high}}$ observed in Model 1 corresponds directly to the localized impingement zones where the high-velocity blood jet aggressively strikes the aneurysm neck or dome. Minimizing these exposed regions is a primary clinical imperative, as abnormally high shear stresses trigger severe endothelial dysfunction and accelerate the degradation of the vascular extracellular matrix via matrix metalloproteinases (MMPs) [4], [27]. This localized enzymatic degradation weakens the structural collagen and elastin fibers within the arterial wall, increasing the probability of catastrophic rupture.

Thus, configurations that successfully suppress the $\mathrm{TAWSS_{high}}$ coverage below the untreated baseline, most notably Model 5 (0.361%), exhibit a highly protective mechanical profile. By dampening the incoming high-velocity blood jet and reducing the impingement forces acting directly against the fragile aneurysm wall, this specific configuration prevents shear-induced biological degradation[6]. Conversely, stents that elevate the high-shear regions beyond the baseline present a detrimental hemodynamic outcome, emphasizing the critical protective mechanism required for mitigating haemorrhagic rupture post-treatment [8].

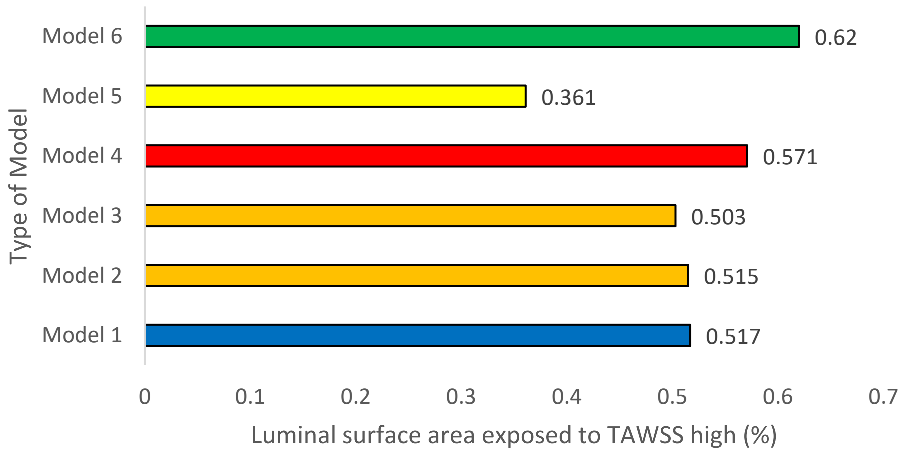

Fig. 10 $TAWSS_{high}$ *(TAWSS > 10 Pa) distribution coverage to luminal surface area of intracranial aneurysm model*

3.3 Limitations

Several modelling assumptions should be considered when interpreting these results. First, the arterial walls were modelled as rigid, neglecting fluid-structure interaction (FSI). Although rigid walls are standard in preliminary CFD studies, this assumption may slightly overestimate peak shear stresses. Second, blood was assumed to be a Newtonian fluid; although acceptable for large arteries, incorporating non-Newtonian models could yield different shear stress values in regions of high flow stasis. Third, generic boundary conditions were applied rather than patient-specific flow waveforms. Finally, the present study focused primarily on TAWSS and velocity fields. Incorporating multidirectional indices such as the Oscillatory Shear Index (OSI) and Relative Residence Time (RRT), as well as modelling biological processes like thrombus formation, remains an area for future work.

4. Conclusions

This study computationally investigated the hemodynamic alterations induced by various flow diverter stent configurations in an intracranial aneurysm model, aiming to identify designs that effectively normalize the Time-Averaged Wall Shear Stress (TAWSS) and mitigate rupture risks. The evaluation critically assessed the balance of three distinct shear zones: $\text{TAWSS}_{\text{normal}}$, which is essential for maintaining physiological endothelial health; $\text{TAWSS}_{\text{low}}$, which is associated with excessive flow stagnation and inflammatory cell infiltration; and $\text{TAWSS}_{\text{high}}$ (> 10 Pa), which drives the aggressive enzymatic degradation of the structural extracellular matrix. The findings demonstrated that geometric stent configurations profoundly dictate local hemodynamics. Notably, Model 5 emerged as the most mechanically protective design. Compared to the detrimental high-shear impingement zones observed in the untreated baseline, Model 5 successfully minimized the $\text{TAWSS}_{\text{high}}$ luminal surface coverage to a mere 0.361%. By efficiently dampening the incoming blood jet and optimizing the distribution of low and normal shear regions, this configuration prevents aggressive endothelial dysfunction far more effectively than the other evaluated models.

The significant variation in hemodynamic outcomes across the tested configurations underscores the critical importance of evaluating specific stent designs prior to clinical deployment, as suboptimal geometries may fail to mitigate, or even inadvertently exacerbate, dangerous wall stresses. To further advance this research, future studies should consider the integration of fluid-structure interaction (FSI) to account for the hyperplastic properties and compliance of the aneurysm wall, which were assumed to be rigid in the current model. Additionally, expanding the investigation to include a wider array of patient-specific anatomical variations and modeling the long-term biological processes of endothelialisation will significantly enhance the predictive accuracy of these hemodynamic simulations, ultimately guiding safer and more personalized endovascular interventions.

Acknowledgement

This research was supported by the Ministry of Higher Education (MOHE) through the Fundamental Research Grant Scheme (FRGS) (FRGS/1/2024/TK10/UTHM/02/6).

Conflict of Interest

Authors declare that there is no conflict of interest regarding the publication of the paper.

Author Contribution

The authors confirm contribution to the paper as follows: ***study conception and design:*** *Muhammad Affiq Syukri Arafat, Nor Adrian Nor Salim, Nur Amani Hanis Roseman;* ***data collection:*** *Muhammad Affiq Syukri Arafat;* ***analysis and interpretation of results:*** *Muhammad Affiq Syukri Arafat;* ***draft manuscript preparation:*** *Muhammad Affiq Syukri Arafat, Nur Amani Hanis Roseman. All authors reviewed the results and approved the final version of the manuscript.*

References

[1] Linkai Jing, Jingru Zhong, Jian Liu, Xinjian Yang, Nikhil Paliwal, Hui Meng, Shengzhang Wang & Ying Zhang (2016) Hemodynamic Effect of Flow Diverter and Coils in Treatment of Large and Giant Intracranial Aneurysms, *World Neurosurgery, 89,* 199–207,https://doi.org/10.1016/j.wneu.2016.01.079

[2] Hailin Zhang, Li Li, F. Miao, J. Yu, Baoyuan Zhou & Yawen Pan (2022) Computational fluid dynamics analysis of intracranial aneurysms treated with flow diverters: A case report, *Neurochirurgie, 68(2),* 235–238, https;//doi.org/10.1016/j.neuchi.2021.03.007

[3] Yuya Uchiyama, Soichiro Fujimura, Hiroyuki Takao, Takashi Suzuki, Toshihiro Ishibashi, Katharina Otani, Kostadin Karagiozov, Koji Fukudome, Hideki Yamamoto, Makoto Yamamoto & Yuichi Murayam (2022) Role of patient-specific blood properties in computational fluid dynamics simulation of flow diverter deployed cerebral aneurysms, *Technology & Health Care, 30(4)*, 839–850, https://doi.org/10.3233/THC-213216

[4] Anqiqng Sun, Chengcheng Zhao, Zujie Gao, Xiaoyan Deng & Hancheng Qiu (2021) A proposed design of flow diverter and it's hemodynamic validation, *Medicine in Novel Technology and Devices 9,* 100049, https://doi.org/10.1016/j.medntd.2020.100049

[5] Farouk Mezali, Khatir Naima, Saida Benmamar & Abdelkrim Liazid (2023) Study and modeling of the thrombosis of small cerebral aneurysms, with and without flow diverter, by the lattice Boltzmann method, *Computer. Methods and Programs in Biomedicine, 233,* 107456, https://doi.org/10.1016/j.cmpb.2023.107456

[6] Hui Meng, Vince M. Tutino, Jianping Xiang & AJAJoN Siddiqui (2014) High WSS or Low WSS? Complex Interactions of Hemodynamics with Intracranial Aneurysm Initiation, Growth, and Rupture: Toward a Unifying Hypothesis, *American Journal of Neuroradiology, 35(7),* https://doi.org/10.3174/ajnr.A3558.

[7] Nan Lv, Christof Karmonik, Shiyue Chen, Xinrui Wang, Yibin Fang, Qinghai Huang & Jianmin Liu (2020) Wall Enhancement, Hemodynamics, and Morphology in Unruptured Intracranial Aneurysms with High Rupture Risk, *Translational stroke research*, *11*(5), 882-889, https://doi.org/10.1007/s12975-020-00782-4

[8] Augustus Fava Sanches, Suprosanna Shit, Yigit Özpeynirci & Thomas Liebig (2022) CFD to Quantify Idealized Intra-Aneurysmal Blood Flow in Response to Regular and Flow Diverter Stent Treatment, *Fluids 7(8),* 254, https://doi.org/10.3390/fluids7080254

[9] Ahmad Faiz Mat Zin, Zin, Ahmad Faiz Mat, Ishkrizat Taib, Muhammad Affiq Syukri Arafat, Nur Amani Hanis Roseman, Muhammad Afiq Mohd Nazri, Muhammad Afif Rifaie Aziz, Muhamad Zaqwan Az-Zikry Norzaidey, Muhammad Sufi Roslan, Takahisa Yamamoto, Awaludin Martin & Mohd Zainizam Mazlan (2025) Hemodynamic Analyses of Different Stent Strut Configurations in the Carotid Artery, *International Journal of Integrated Engineering*, *17*(4), 259-273, https://doi.org/10.30880/ijie.2025.17.04.023

[10] Rico P. J. (2024). Hemodynamic Modelling and Simulation of Flow Diverters for Intracranial Aneurysm Treatment. [Doctoral dissertation, Université Paris sciences et lettres]. HAL Portal theses.

[11] Yasuyuki Umeda, Fujimaro Ishida, Masanori Tsuji, Kazuhiro Furukawa, Masato Shiba, Ryuta Yasuda, Naoki Toma, Hiroshi Sakaida & Hidenori Suzuki (2017) Computational fluid dynamics (CFD) using porous media modeling predicts recurrence after coiling of cerebral aneurysms, *PLOS ONE, 12(12),* e0190222, https://doi.org/10.1371/journal.pone.0190222

[12] Burcu Ramazanli, Oyku Yagmur, Efe Cesur Sarioglu & Huseyin Enes Salman (2025) Modeling Techniques and Boundary Conditions in Abdominal Aortic Aneurysm Analysis: Latest Developments in Simulation and Integration of Machine Learning and Data-Driven Approaches, *Bioengineering 12(5),* 437, https://doi.org/10.3390/bioengineering12050437

[13] Haveena Anbananthan, Phani Kumari Paritala, Jessica Benitez Mendieta, Han Yu, Tiago Guerzet Sardenberg Lima, Zoe Dettrick, Ee Shern Liang, Alan Coulthard, Zhi-Yong Li & Craig Winter (2025) Haemodynamic characteristics of thin-walled regions in intracranial aneurysms: intraoperative imaging and CFD analysis, *Acta Neurochirurgica*, *167*(1), 238, https://doi.org/10.1007/s00701-025-06660-y

[14] Michael Gaub Greg Murtha, Molly Lafuente, Matthew Webb, Anqi Luo, Lee A. Birnbaum, Justin R. Mascitelli & Fadi Al Saiegh (2024) Flow Diversion for Endovascular Treatment of Intracranial Aneurysms: Past, Present, and Future Directions, *Journal of Clinical Medicine*, *13*(14), 4167, https://doi.org/10.3390/jcm13144167

[15] Muhammad Affiq Syukri Arafat, Nor Adrian Nor Salim, Mohd Syahar Mohd Shawal & Mohd Rosdzimin Abdul Rahman (2025) Computational Study on the Hemodynamic Analysis of Intracranial Aneurysms using Flow Diverter Stents, *International Journal of Integrated Engineering*, *17*(8), 285-300, https://doi.org/10.30880/ijie.2025.17.08.024

[16] Yunling Long, Hongyu Yu, Zhizheng Zhuo, Ying Zhang, Yang Wang, Xinjian Yang & Haiyun Li (2014) A geometric scaling model for assessing the impact of aneurysm size ratio on hemodynamic characteristics, *BioMedical Engineering OnLine*, *13*(1), 17, https://doi.org/10.1186/1475-925X-13-17

[17] Yujie Li, David I. Verrelli, William Yang, Yi Qian & Winston Chong (2020) A pilot validation of CFD model results against PIV observations of haemodynamics in intracranial aneurysms treated with flow-diverting stents, *Journal of biomechanics*, *100*, 109590, https://doi.org/10.1016/j.jbiomech.2019.109590

[18] Sunghan Kim, Hyeondong Yang, Ineui Hong, Je Hoon Oh & Yong Bae Kim (2021) Computational Study of Hemodynamic Changes Induced by Overlapping and Compacting of Stents and Flow Diverter in Cerebral Aneurysms, *Frontiers in Neurology*, *12*, 705841, https://doi.org/10.3389/fneur.2021.705841

[19] Borja Catalán-Echeverría, Michael E. Kelly, Lissa Peeling, Donald Bergstrom, Xiongbiao Chen & Mauro Malvè (2019) CFD-Based Comparison Study of a New Flow Diverting Stent and Commercially-Available Ones for the Treatment of Cerebral Aneurysms, *Applied Sciences*, *9*(7), 1341, https://doi.org/10.3390/app9071341

[20] Benjamin Csippa, Levente Sándor, Gábor Závodszky, István Szikora & György Paál (2024) Comparison of Flow Reduction Efficacy of Nominal and Oversized Flow Diverters Using a Novel Measurement-assisted in Silico Method, *Clinical Neuroradiology*, *34*(3), 675-684, https://doi.org/10.1007/s00062-024-01404-4

[21] Maria Antonietta Boniforti, Roberto Magini & Tania Orosco Salinas (2023) Hemodynamic Investigation of the Flow Diverter Treatment of Intracranial Aneurysm, *Fluids, 8(7),* 189, https://doi.org/10.3390/fluids8070189

[22] Asgari, H. (2022). Numerical Simulations of Bifurcation Cerebral Aneurysm Hemodynamics [Doctoral dissertation, University of British Columbia]. UBC Theses and Dissertations.

[23] Xiaolin Wu, Stefanie Gürzing, Christiaan Schinkel, Merel Toussaint, Romana Perinajová, Pim Van Ooij & Saša Kenjereš (2022) Hemodynamic Study of a Patient-Specific Intracranial Aneurysm: Comparative Assessment of Tomographic PIV, Stereoscopic PIV, In Vivo MRI and Computational Fluid Dynamics, *Cardiovascular Engineering and Technology*, *13*(3), 428-442, https://doi.org/10.1007/s13239-021-00583-2

[24] Lim Sheh Hong, Mohd Azrul Hisham Mohd Adib, Mohd Shafie Abdullah, Nur Hartini Mohd Taib, Radhiana Hassan & Azian Abd Aziz (2020) Study of Extracted Geometry Effect on Patient-Specific Cerebral Aneurysm Model with Different Threshold Coefficient (Cthres), *CFD Letters, 12(10),* 1–14, https://doi.org/10.37934/cfdl.12.10.114

[25] Xiaochang Leng, Yang Wang, Jing Xu, Yeqing Jiang, Xiaolong Zhang & Jianping Xiang (2018) Numerical simulation of patient-specific endovascular stenting and coiling for intracranial aneurysm surgical planning, *Journal of translational medicine*, *16*(1), 208, https://doi.org/10.1186/s12967-018-1573-9

[26] Castro, M. A., Putman, C. M., & Cebral, J. R. (2006) Computational fluid dynamics modeling of intracranial aneurysms: effects of parent artery segmentation on intra-aneurysmal hemodynamics. *American Journal of Neuroradiology*, *27*(8), 1703-1709, https://www.ajnr.org/content/27/8/1703.full

[27] Sima Baheri Islami, Mike Wesolowski, William Revell & Xiongbiao Chen (2021) Virtual Reality Visualization of CFD Simulated Blood Flow in Cerebral Aneurysms Treated with Flow Diverter Stents, *Applied Sciences*, *11*(17), 8082, https://doi.org/10.3390/app11178082